Geophysical Journal International

Geophys. J. Int. (2023) **235,** 1420–1433
Advance Access publication 2023 August 04
GJI Gravity, Geodesy and Tides

https://doi.org/10.1093/gji/ggad311

The 95 per cent confidence interval for the mean sea-level change rate derived from tide gauge data

Guoquan Wang

Department of Earth and Atmospheric Sciences, University of Houston, Houston, TX 77204*, USA. E-mail: gwang@uh.edu*

Accepted 2023 August 3. Received 2023 August 2; in original form 2023 May 5

SUMMARY

Tide gauge (TG) data are crucial for assessing global sea-level and climate changes, coastal subsidence and inundation. Mean sea-level (MSL) time-series derived from TG data are autocorrelated. The conventional ordinary least-squares regression method provides reasonable estimates of relative sea-level (RSL) change rates (linear trends) but underestimates their uncertainties. In order to cope with the autocorrelation issue, we propose an approach that uses an 'effective sample size' ($N_{\rm eff}$) to estimate the uncertainties ($\pm$95 per cent confidence interval, or 95 per cent CI for short). The method involves decomposing the monthly MSL time-series into three components: a linear trend, a periodic component and a noise time-series. The $N_{\rm eff}$ is calculated according to the autocorrelation function (ACF) of the noise time-series. We present an empirical model that fits an inverse power-law relationship between 95 per cent CI and time span (T) based on 1160 TG data sets globally distributed, where 95 per cent CI $= 179.8T^{-1.29}$. This model provides a valuable tool for projecting the optimal observational time span needed for the desired uncertainty in sea-level rise rate or coastal subsidence rate from TG data. It suggests that a 20-yr TG time-series may result in a 3–5 mm yr^{-1} uncertainty (95 per cent CI) for the RSL change rate, while a 30-yr data set may achieve about 2 mm yr^{-1} uncertainty. To achieve a submillimetre per year ($<$ 1 mm yr^{-1}) uncertainty, approximately 60 yr of TG observations are needed. We also present a Python module (TG_Rate_95CI.py) for implementing the methodology. The Python module and the empirical model have broad applications in global sea-level rise and climate change studies, and coastal environmental and infrastructure planning, as well as Earth science education.

Key words: Sea level change; Statistical methods; Time-series analysis.

1 INTRODUCTION

1.1 Motivation

Coastal areas are home to a significant proportion of the global population. Rising sea level and coastal subsidence have exerted sustained impacts on coastal public and energy infrastructures, coastal ecosystems and their supporting services. Long-term sea-level data from tide gauge (TG) stations are essential for studying the global sea-level rise and climate changes, and a variety of local and regional coastal processes, such as decadal climate variability, coastal subsidence and inundation. Sea level at any location varies due to a wide range of physical processes, such as local and regional meteorological effects, climate variability (e.g. El Niño and La Niña) and long-term trends (e.g. Church & White 2011; Harrison 2002). In this paper, we refer to a series of monthly mean sea-level (MSL) measurements from TG data as the TG time-series. MSL is usually calculated by taking the arithmetic average of hourly data for each calendar month. The TG time-series is often used to calculate site-specific sea-level change rates by fitting a simple line to the data. These rates are essential for understanding the impacts of sea-level rise and coastal subsidence on coastal infrastructure, ecosystems, and their services.

The global mean sea-level (GMSL) change rate is currently around a couple of millimetres per year. The latest Intergovernmental Panel on Climate Change (IPCC) report states that the GMSL change rate was 1.3 $\pm$ 0.7 mm yr^{-1} (rate $\pm$ 90 per cent confidence interval, abbreviated as CI) between 1901 and 1971, which increased to 1.9 $\pm$ 1.0 mm yr^{-1} between 1971 and 2006, and further increased to 3.7 $\pm$ 0.5 mm yr^{-1} between 2006 and 2018 (IPCC 2021). In the Gulf of Mexico, Wang *et al.* (2020) reported an average MSL rise rate of 2.6 mm yr^{-1} over the past half-century with respect to the stable Gulf of Mexico Reference Frame (GOM20). TG records changes in sea level relative to one or more fixed benchmarks located nearby. The rate derived from TG time-series typically contains a component due to oceanography and another due to vertical land movements (VLMs), which can include historic anthropogenic subsidence, long-term natural subsidence, postglacial rebound and

other types of land deformation. The rate of natural subsidence is also at a level of a couple of millimetres per year or even lower (e.g. Zhou *et al.* 2021). Due to the small values of these rates, their uncertainties are crucial for accurately quantifying spatial-temporal variations of sea level and coastal subsidence.

In statistics, there are sophisticated mathematical methods for calculating the linear trend and its uncertainty for stationary time-eries. TG time-eries is often analysd using a least-quares linear regression to estimate the RSL change rate, which determines the potential flooding or erosion of coastal communities. This linear regression is reliable and accurate for estimating the rate for TG data sets that span over 30 yr or more, but it often underestimates the uncertainty for the rate. The cause of the problem is well known: TG time-series are autocorrelated, not stationary, as evidenced by numerous studies (e.g. Harrison 2002; Zervas 2009; Bos *et al.* 2014; Dangendorf *et al.* 2014). Each MSL measurement is not entirely independent of its preceding and subsequent measurements, so each measurement provides less information than an independent or uncorrelated measurement would. As a result, the standard error of the rate, which indicates the reliability (or confidence) of the estimated rate, is frequently underestimated by the conventional least-squares regression. Temporal correlations are frequently found in geophysical signals, especially in the form of power-law noises (e.g. Agnew 1992; Beran 1992; Langbein & Johnson 1997; Langbein 2004; Williams 2008).

Over the past two decades, researchers in the fields of geodesy and coastal engineering have increasingly used Global Navigation Satellite System (GNSS) data to supplement TG data to recover historical VLMs (e.g. Snay *et al.* 2007; Yu & Wang 2016; Zervas *et al.* 2013; Burgette *et al.* 2013; Yang & Francis 2019; Qiao *et al.* 2022). Recently, Wang (2022) developed a robust methodology for calculating the uncertainties of the rates (site velocities) from daily GNSS time-series, using an effective sample size (N_{eff}) to determine the uncertainty of the rate. This methodology provides reasonable uncertainty estimates and has been implemented in a Python programming module (Cornelison & Wang 2022). This paper intends to develop a similar methodology for estimating the uncertainty of the trend of monthly TG time-series. A consistent methodology will allow for comparable uncertainty estimates for the rates of VLMs (from GNSS data) and relative sea-level (RSL) changes (from TG data). Ultimately, this will result in a more reliable estimate of the uncertainty of the absolute sea-level (ASL) change rate.

In this paper, the term uncertainty is used to refer to the range of values within which a parameter is likely to fall. The standard error of the rate obtained from linear regression for a stationary time-series is equivalent to a 68 per cent CI. A 90 per cent CI can be estimated as 1.64 times the standard error, and 95 per cent CI can be estimated by 1.96 times the standard error (Box *et al.* 2008). Throughout this paper, we will use a ± 95 per cent CI as our primary measure of the uncertainty. This interval is widely considered to provide a very likely range of values, and will allow us to make more conservative estimates of our uncertainty.

1.2 Common problems

Sea-level rise rate is often quantified by a linear rate derived from the monthly or yearly TG time-series. The most commonly used form of linear regression is the ordinary least-squares (OLS) regression. The monthly MSL time-series (y_i) can be modelled by:

$$y_i = a + bt_i + R_i, \tag{1}$$

where a is the intercept of the regression line, b represents the rate (linear trend or slope) of the linear regression and R_i is the residual time-series. OLS regression assumes that the residual time-series is white, with no temporal correlation among the residuals. The linear trend line can be described as:

$$L_i = a + bt_i. \tag{2}$$

If the residual time-series (R_i) is stationary, the standard error (SE_b) for the rate (b) can be calculated according to the following equation (Wilks 2006):

$$\text{SE}_b = \frac{s}{\sqrt{N}} \times \frac{1}{\sigma_t}, \tag{3}$$

where s is the standard deviation of the residual time-series,

$$s = \sqrt{\frac{\sum R_i^2}{N-2}}, \tag{4}$$

σ_t is the standard deviation of the t_i (monthly decimal year series); $\frac{1}{\sigma_t}$ merely serves to scale the values. For t_i spanning over T years, $\sigma_t \approx T/(2\sqrt{3})$ (Wang 2022). The unit of SE_b is consistent with the unit of the rate.

For a stationary time-series, SE_b is a reliable indicator of the uncertainty in the estimate of b. However, for TG data, even after removing the average seasonal cycles, the R_i is not stationary. This results in a smaller number of independent measurements contributing to the standard error (SE_b, eq. 3). As a consequence, the SE_b calculated using the total sample number 'N' can be unrealistically small, although the rate itself (b) is often accurate (Box *et al.* 2008).

1.3 Current approaches

To cope with the autocorrelation issue in TG data sets, researchers have employed various stochastic models to model the residual time-series (R_i), including white noise, autoregressive noise (first order or higher orders), autoregressive-moving-average noise, autoregressive fractionally integrated noise, first-order Gauss–Markov noise and generalized Gauss Markov noise (Zervas 2009; Nerem *et al.* 2010; Burgette *et al.* 2013; Bos *et al.* 2014). In general, the uncertainty for the rate can be estimated according to the modelled noise time-series. However, different methods may involve different models, parameter adjustments and calibrations, resulting in different estimates for the rate uncertainty (see Fig. 1).

The Permanent Service for Mean Sea Level (PSMSL) is a global repository for MSL data collected from TG stations around the world (Holgate *et al.* 2013). Prior to 2015, PSMSL relied on a simple linear regression to calculate the linear trend and estimate its uncertainty for yearly TG time-series. However, PSMSL changed its data processing strategy in 2015, and now uses monthly MSL time-series with trend and uncertainty determined using an Integrated Generalized Gauss Markov stochastic model (PSMSL 2022b). In the United States, the Center for Operational Oceanographic Products and Services (CO-OPS) at the National Oceanic and Atmospheric Administration (NOAA) operates the national water level network and publishes the data. CO-OPS employs a first-order autoregressive model AR(1) to model the residual time-series and estimates the 95 per cent CI for the rate of RSL change (Zervas 2001, 2009). The variations in estimates among different methods could lead to confusion and misunderstandings within the broad TG data user community.

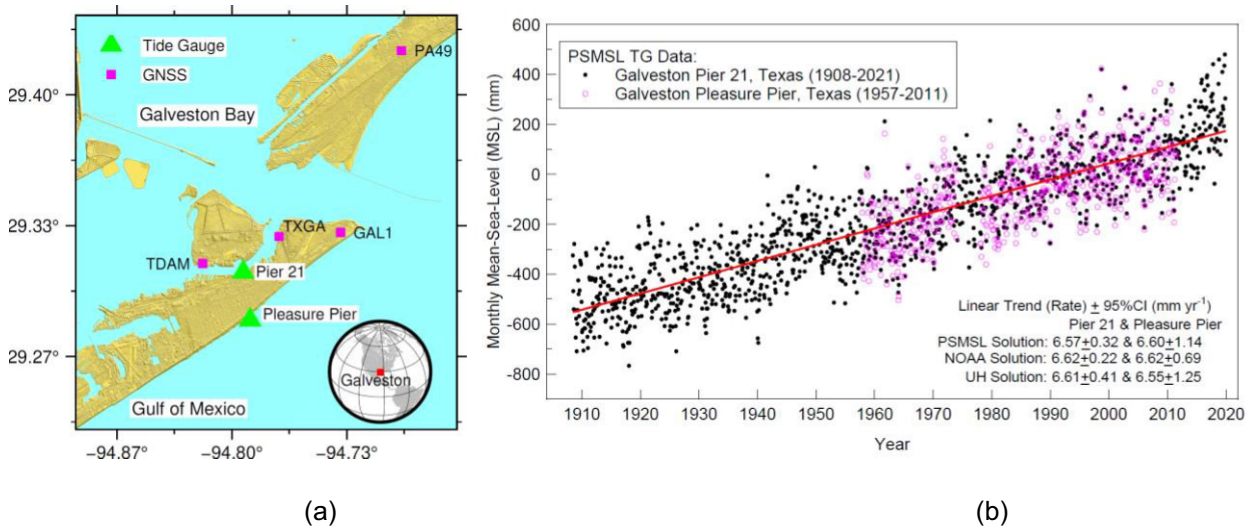

Figure 1. (a) Location of two TGs on Galveston Island, Texas: Pleasure Pier (PSMSL ID: 828) and Pier 21 (PSMSL ID: 161). (b) Monthly MSL time-series at the two TG sites. The rates and their uncertainties (±95 per cent CI) at each site provided by PSMSL and NOAA are marked in the figure. Additionally, the rates and their uncertainties estimated using the methodology presented in this paper are also marked on the figure, labelled as 'UH solution', which used the PSMSL released data.

Fig. 1 depicts the monthly MSL data collected from two long-term TG stations situated in close proximity to each other on Galveston Island, Texas coast. One TG station, located at Galveston Pier 21, has been operational for about 118 yr (1904–2021), while the other, located at Pleasure Pier, has an observational history of about 55 yr (1957–2011). The Pier 21 TG station's early measurements from 1904 to 1907 are not included in the PSMSL data but are available in the NOAA data. The Pier 21 TG station is situated in Galveston Bay, a back-barrier coastal lagoon between the Galveston barrier island and Pelican Island, while the Pleasure Pier TG is on the Gulf side, about 3 km away (Fig. 1a). The RSL change rates and their corresponding uncertainties (as of the end of 2021) provided by PSMSL and NOAA are marked in Fig. 1(b). Additionally, the rates and their uncertainties obtained from the University of Houston (UH) method, introduced in this study, are shown for comparison purposes. While NOAA quantifies the uncertainty of the trend using ± 95 per cent CI, PSMSL uses ± SE (the corrected standard error of the rate), which is approximately ± 68 per cent CI. All methods yield RSL change rates of approximately 6.6 mm yr^{-1} at both sites, with differences not exceeding 0.1 mm yr^{-1}. The focus of this study is on the rates' uncertainties, and hence the rates themselves will not be discussed further.

It is noteworthy that the NOAA data have undergone adjustments made by their experts. These adjustments involve removing site-specific average seasonal cycles, which helps eliminate temporally correlated noises originating from sea level, land surface and instruments. The methodology and the 12 calendar monthly means for each of the U.S. TG stations are explained in Zervas (2009). Fig. 2 illustrates a comparison between the TG data at Galveston Pleasure Pier (1957–2011) released by PSMSL and NOAA (seasonally adjusted) for calculating the rate and its corresponding 95 per cent CI. The rate and its 95 per cent CI obtained from the UH method are marked in the figure. The RSL change rates obtained from both data sources are nearly identical (6.62 mm yr^{-1} vs 6.55 mm yr^{-1}). However, the uncertainty estimation using NOAA data (±0.88 mm yr^{-1}) is lower compared to the PSMSL data (±1.25 mm yr^{-1}). The difference could be remarkable for applications that require high precision.

2 METHODS

2.1 Time-series decomposition

The monthly MSL time-series (y_i) can be decomposed into three components:

$$y_i = L_i + P_i + r_i. \tag{5}$$

L_i is obtained by applying a linear regression on the entire TG time-series (eq. 2). P_i represents the periodic component, the sum of the periodicities with different frequencies. r_i represents the noise component. Fig. 3 shows an example of TG time-series decomposition at the Galveston Pleasure Pier (1957–2011). The original monthly TG time-series is from PSMSL. The details of the decomposition process will be addressed in the following.

In the method, presented in Wang (2022) for estimating the 95 per cent CI for the rate of daily GNSS time-series, the periodic component only includes period- and amplitude-fixed seasonal (annual and semi-annual) cycles. This is reasonable for GNSS measurements with a history within a couple of decades. However, TG time-series often span over multidecades to a century, or even longer, and comprise signals with interannual periods and changing amplitudes (e.g. Zhang & Church 2012). A seasonal model is unable to fully capture the deterministic portion of the TG data, as all periodic signals should be considered part of the deterministic component. In this study, P_i and r_i are obtained by conducting the singular spectrum analysis (SSA) on the de-linear trended TG time-series (R_i):

$$R_i = P_i + r_i. \tag{6}$$

SSA is a widely used nonparametric technique for spectral estimation of time-series. The fundamental idea behind SSA is to decompose a given time-series into a finite number of additive components, each with a distinct period or frequency (Golyandina & Zhigljavsky 2020). These components are obtained by constructing a set of matrices from the original time-series and decomposing them into eigenvalues and eigenvectors using principal component analysis. The original time-series is recoverable by adding together all the periodicities. In this study, we employ a Python module for SSA developed by Faouzi & Janati (2020).

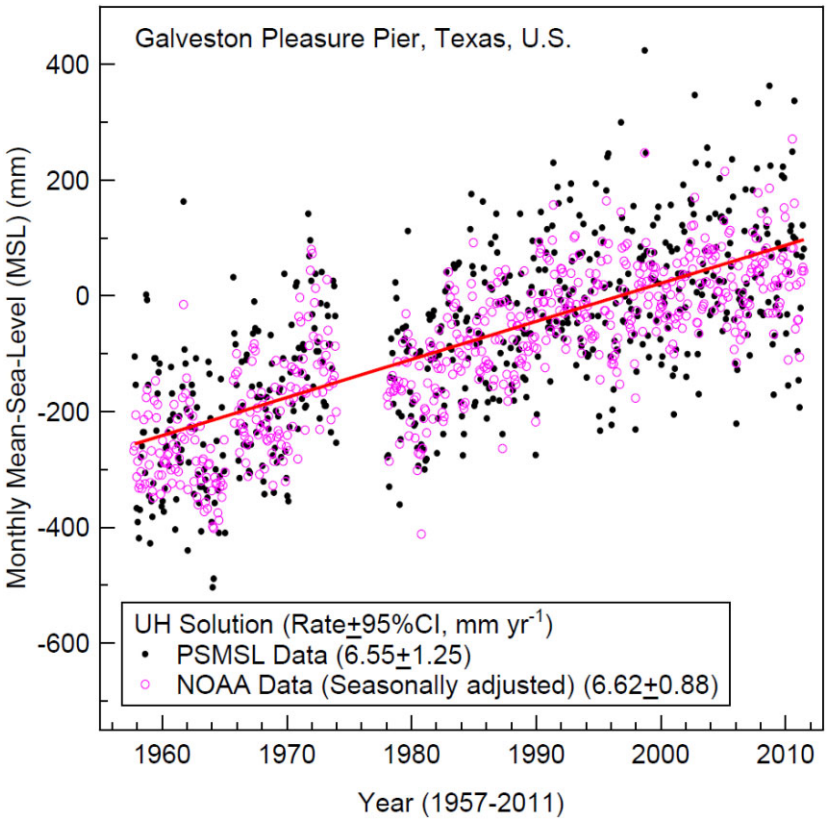

Figure 2. Comparison of monthly MSL data recorded at Galveston Pleasure Pier (1957–2011) as released by PSMSL (PSMSL 2022a) and NOAA (NOAA 2022a). NOAA has removed a site-specific average seasonal cycle for each MSL time-series (Zervas 2009).

Fig. 4 displays the first 10 periodicities (F_0 to F_9) obtained using the SSA method for the residual time-series (R_i) of the TG data at Galveston Pleasure Pier. Precisely grouping the SSA results by their periods can be challenging, but in this study, there is no need to perform such grouping since only the sum of periodicities is used in the decomposition (eq. 5). Fig. 4(a) illustrates the SSA results for the NOAA data, in which the average seasonal cycle has been removed by NOAA experts. Fig. 4(b) illustrates the SSA results for the PSMSL data. Annual and half-annual variabilities are significant in the PSMSL data, as expected. There is a remarkable 19-yr (approximately) cycle in both PSML and NOAA data sets. The cycle is believed to represent the Metonic cycle, which is 18.61 yr, and influences long-period (multidecadal) tidal amplitudes globally (e.g. Peng *et al.* 2019). The 19-yr cycle is an indicator of the long-term variations in the orbit of the moon. Moreover, elements with multiyear periods (e.g. 2–6-yr) primarily average out the effects of local weather and oceanographic conditions due to multiyear climate variability, such as El Niño, La Niña and the Pacific Decadal Oscillation.

The SSA module sorts the periodic elements according to their amplitudes, with larger amplitudes appearing first. In our investigation of TG data, we found that periodicities beyond the 10th element often have amplitudes of less than 15 mm, and therefore make only a small contribution to the total periodic component (P_i). To determine the optimal number of elements to include, we compared the SSA results for different element sets ranging from the first 10 to the first 20 elements. We found that the differences in the final 95 per cent CI estimates were negligible, with a statistical significance of less than 0.1 mm yr^{-1}. Therefore, in this study, we estimated P_i by summing the amplitudes of the first 15 elements (F_0 to F_{14}) of the SSA results:

$$P_i = \sum_{j=0}^{j=14} F_j(i). \tag{7}$$

The noise component is obtained by:

$$r_i = R_i - P_i. \tag{8}$$

Data gaps are a common occurrence in TG time-series and are often caused by temporary equipment failure in the field. To apply SSA, a continuous time-series is required, meaning that the data gaps in the residual time-series (R_i) must be filled prior to conducting spectrum analysis. In this study, the Python function 'random.choice' was used to randomly select measurements from the R_i time-series to fill the gaps (see Figs 3a and b). The potential impact of data gaps on the estimation of 95 per cent CI will be discussed in the following section.

2.2 Effective sample size

'Effective sample size' (N_{eff}) is a term used in statistics to represent the independent samples among autocorrelated measurements. The concept of N_{eff} has been frequently used in studying the correlations of geophysical data sets, including oceanography, meteorology, geodesy and seismology, among others (e.g. Taubenheim 1974; Thiébaux & Zwiers 1984; Kass *et al.* 1998; Kermarrec *et al.* 2022; Wang 2022). In this study, we will use N_{eff} to evaluate the impact of the autocorrelation on the statistical analysis of the TG data set.

Autocorrelation function (ACF) and partial autocorrelation function (PACF) are often used for assessing the temporal correlations

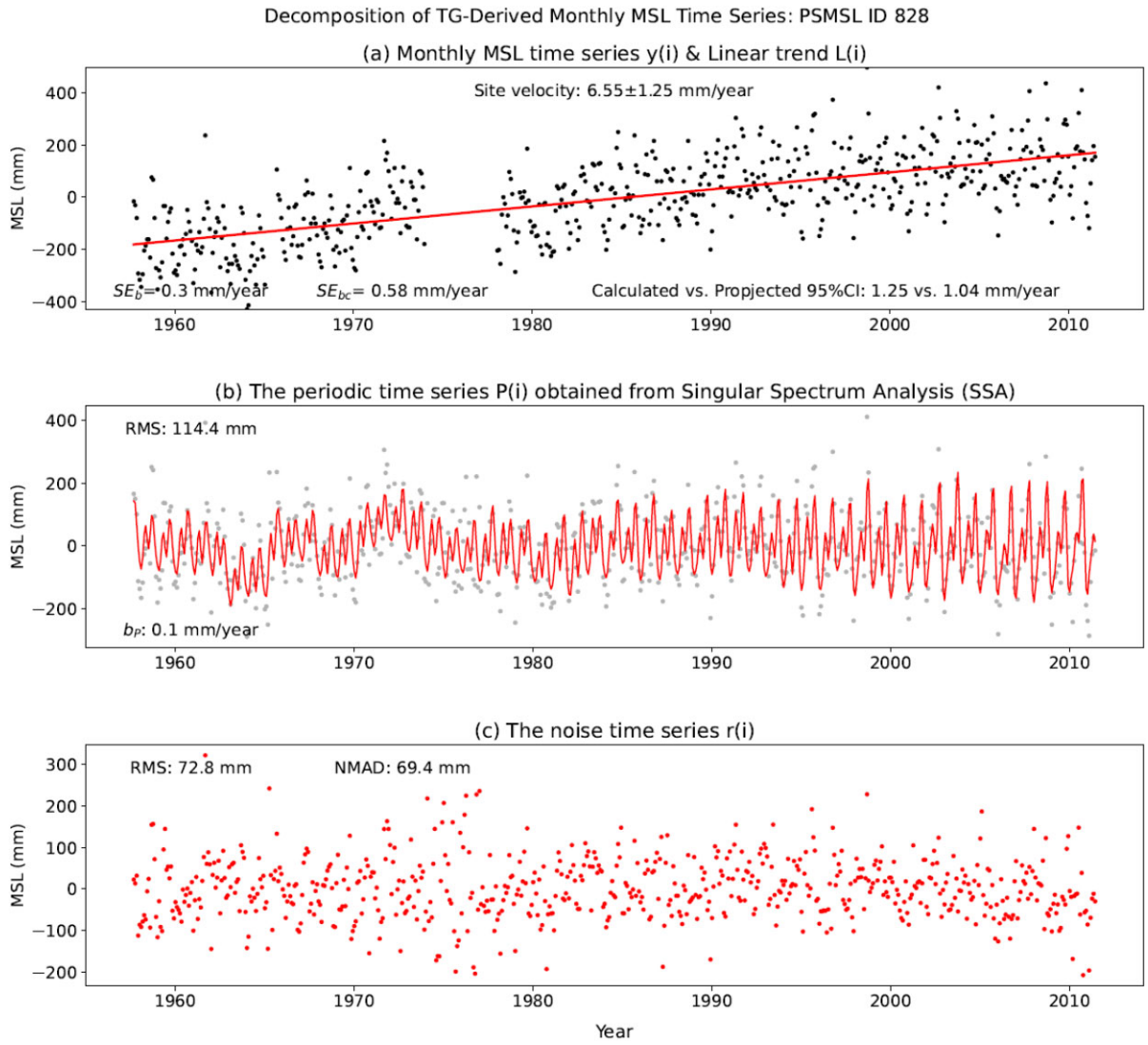

Figure 3. Decomposition of the TG time-series at Galveston Pleasure Pier according to eq. (5). The periodic time-series in subfigure (*b*) is obtained from SSA on the monthly MSL time-series after removing the linear trend.

among observations. The ACF measures the correlation between the time-series and its own lagged values, while the PACF measures the correlation of a series with itself at increasing lags, with the correlations at intervening lags removed. By examining the shape and magnitude of the ACF and PACF plots, we can gain insight into the nature of the temporal correlations in the data. To model the noise time-series (r_i), we can use an autoregressive model AR(p),

$$r_i = \varphi_0 + \varphi_1 r_{i-1} + \varphi_2 r_{i-2} + \cdots + \varphi_p r_{i-p} + \varepsilon_i \quad (9)$$

where p is the order of the AR model. The AR(p) model assumes that the current value of the series depends linearly on the past p values, plus a white noise term (ε_i). The parameters of the AR(p) model can be estimated using various techniques, such as maximum likelihood or least squares. A reasonable order of the AR(p) model can be estimated according to the PACF of the noise time-series (r_i). φ_k is the PACF of the noise (r_i) at lag k, PACF(k) =φ_k. $\varphi_k \approx 0$ for $k > p$. ε_i can be approached by a white noise series with zero mean and the same variance (σ^2) with the noise time-series (r_i).

Fig. 5(a) depicts the PACF of the noise time-series (r_i) of the TG data at Galveston Pier 21 (1908–2021). The original MSL time-series is from PSMSL. Partial autocorrelation coefficients that are significantly different from zero indicate lagged terms of the AR process (eq. 9). The dashed lines depict the ± 95 per cent confidence interval of the estimated PACF, which is determined by $\pm 1.96/\sqrt{N}$. N is the number of total measurements. The partial-correlation coefficients within the ± 95 per cent CI are statistically close to zero. The PACF has about four significant lags. Accordingly, a fourth-order AR model may work well to model the noise time-series in the TG data set at Galveston Pier 21.

A range of AR models from AR(1) to AR(5) have been used by previous researchers to model the noises superimposed into TG data (e.g. Hughes & Williams 2010; Nerem *et al.* 2010; Church & White 2011; Hay *et al.* 2013; Bos *et al.* 2014). In practice, determining the appropriate order for an autoregressive model using the PACF can be a challenge, and the computation for PACF can be slow as it requires estimating a set of OLS regressions. However, the methodology proposed in this paper does not require calculating the PACF or determining the order of the autoregressive model.

Researchers in statistics have found that, for a high-order autoregressive process, the N_{eff} can be estimated by correcting the original sample size (N) with a coefficient called autocorrelation time (τ)

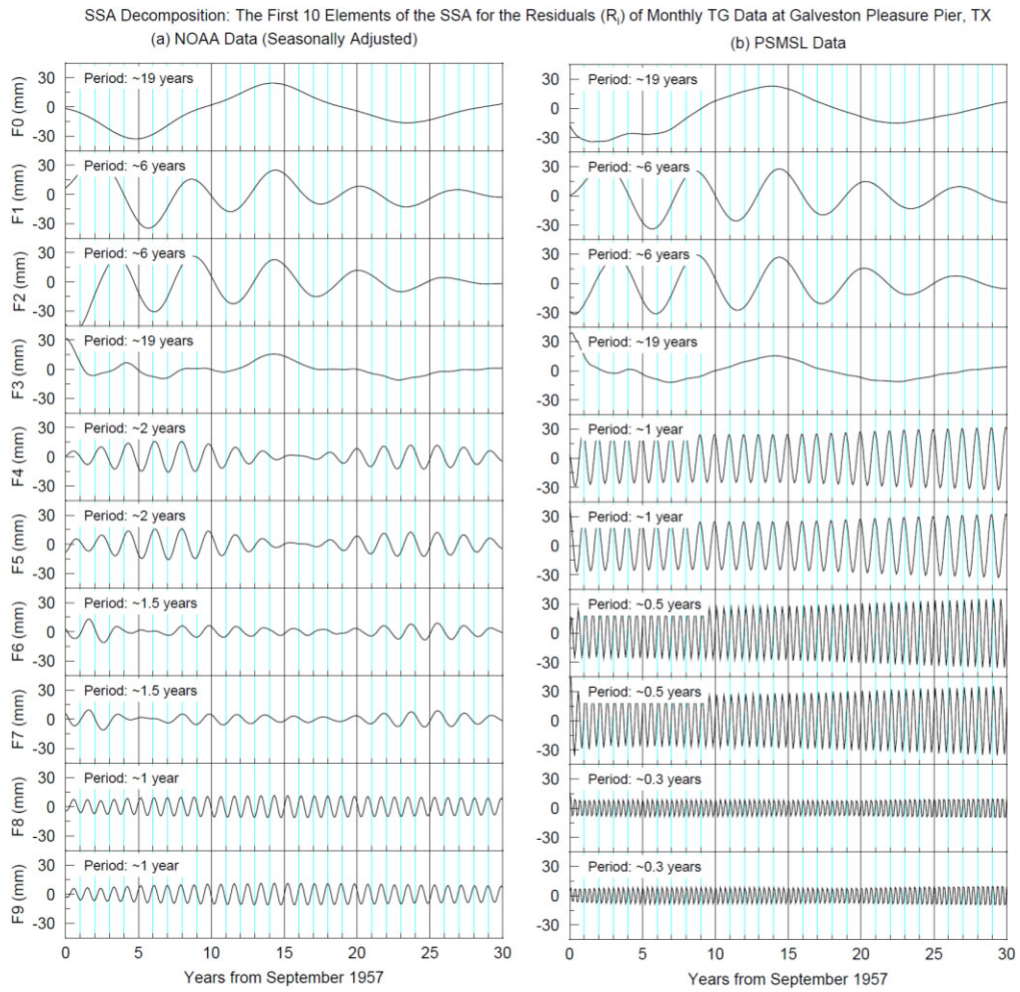

Figure 4. Results of the SSA on the detrended monthly MSL data (R_i) at Galveston Pleasure Pier (1957–2011). (a) The first 10 elements of the SSA results for the NOAA data (seasonally adjusted) and (b) the first 10 elements of the SSA results for the PSMSL data.

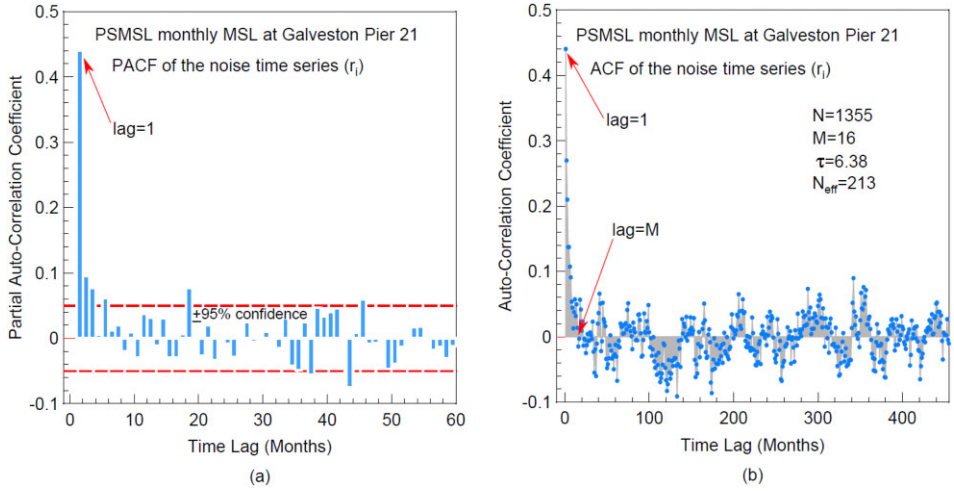

Figure 5. (a) The PACF and (b) ACF for the noise time-series (r_i) of the monthly MSL data at Galveston Pier 21 (PSMSL data). Dashed lines in (a) represent the ± 95 per cent CI of the PACF, estimated by $\pm 1.96/\sqrt{N}$, where N is the number of TG measurements.

(Straatsma *et al.* 1986; Geyer 1992; Thompson 2010):

$$N_{\text{eff}} = \frac{N}{\tau}. \tag{10}$$

For an autocorrelated time-series, τ can be estimated by:

$$\tau = 1 + 2 \times \sum_{k=1}^{\infty} \rho(k), \tag{11}$$

where $\rho(k)$ is the lag-k ACF of the noise time-series (r_i in eq. 8). The autocorrelation time (τ) reflects the rate at which the correlation between observations decays as the time lag increases. When τ is high, it indicates that the time-series is strongly correlated and that the N_{eff} is lower than the actual sample size. In contrast, a low τ suggests that the time-series is weakly correlated, and the N_{eff} is closer to the actual sample size. Correcting for the sample size is crucial when computing statistical measures, such as standard errors, confidence intervals and hypothesis tests. By estimating N_{eff}, we can obtain more accurate statistical estimates and avoid underestimating the uncertainty of the results.

Fig. 5(b) illustrates the ACF of the noise time-series (r_i) recorded at Galveston Pier 21 (1908–2021). The ACF initially decays gradually towards zero for a few lags and then fluctuates around the zero-axis. The overall decay of the ACF reflects weaker statistical relationships between measurements that are further apart in time. The ACF indicates that the coefficient after the lag M is an undulating function of the time span that crosses the zero-axis. The areas below and above the x-axis are approximately equal, indicating that $\sum_{i=M+1}^{\infty} \rho(k) \approx 0$. Therefore, $\sum_{i=1}^{M} \rho(k)$ is a reasonable approximation of $\sum_{i=1}^{\infty} \rho(k)$. Consequently, the infinite sum can be truncated at the last lag M, where the sum of $\rho(M)$ and $\rho(M+1)$ is greater than or equal to zero. The practice of truncating $\rho(k)$ to lag M has been a well-established method used by previous researchers (e.g. Thiébaux & Zwiers 1984; Geyer 1992). In summary, a realistic standard error of the linear trend (SE_b, eq. 3) can be estimated using N_{eff}, instead of N:

$$\text{SE}_{bc} \approx \frac{s}{\sqrt{N_{\text{eff}}}} \times \frac{1}{\sigma_t} = \text{SE}_b \times \sqrt{\tau}. \tag{12}$$

2.3 Determination of the 95 per cent CI

As previously mentioned, the uncertainty of the linear trend (b) is determined by the residual time-series (R_i), which is a combination of deterministic variations (P_i) and noises (r_i) (eq. 6). In some cases, the periodic component can exhibit a notable linear trend that drifts away from zero. Fig. 6 illustrates the MSL data set (1948–2021) at Rockport, Texas, in Aransas Bay, where a nonlinear trend line is plotted to display the decadal-scale variations of the TG data. The nonlinear trend line is obtained using locally weighted scatterplot smoothing (LOWESS, Cleveland 1981). The plot reveals several decadal-scale steps or shifts that indicate an acceleration or deceleration of sea-level change or land-surface elevation change. According to Zhou *et al.* (2021), the accelerated RSL rise that occurred from 1988 to 2000 was caused by the anthropogenic subsidence associated with excessive groundwater withdrawal in this area during that period. The anthropogenic subsidence ceased since the 2000 s because of the reduced pumping. The upward shift of the nonlinear trend since 2010 indicates that the ongoing sea-level rise is accelerating, which is also observed in satellite altimetry data (e.g. Hamlington *et al.* 2020).

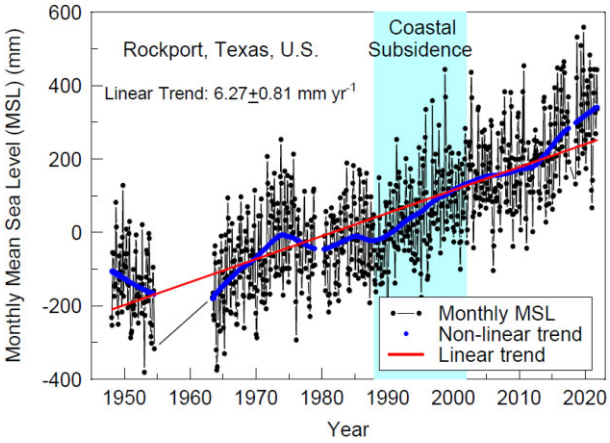

Figure 6. Monthly MSL recorded by the TG at Rockport, Texas, showing a significant long-period nonlinear trend.

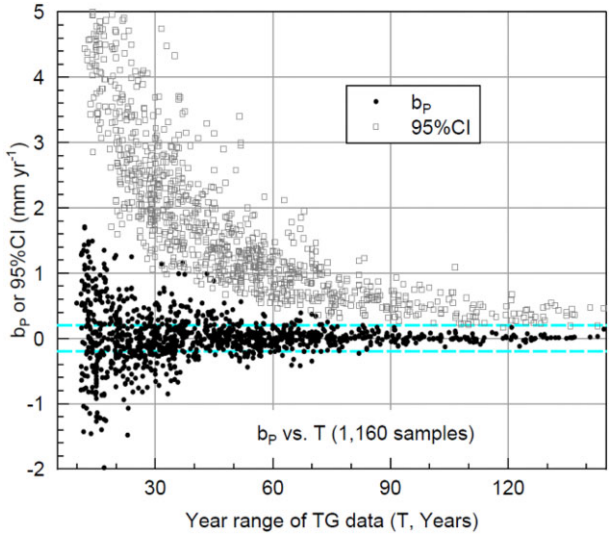

Figure 7. Plot illustrating how the line trend (b_P) of the periodic component (P_i) contributes to the final 95 per cent CI (see eq. 13). The dashed lines indicate $\pm$ 0.2 mm yr^{-1} uncertainty.

TG data may exhibit random walk noises that can have a significant effect on the rate uncertainty (e.g. Langbein 2012). Bos *et al.* (2014) reported that 13 per cent to 17 per cent of the PSMSL data sets contained a random walk component. Those temporal shifts and random walk noises would be reflected in the periodic component (P_i) as long-period signals (decadal to multidecadal), which can result in a slight linear trend (b_P) in the periodic time-series (P_i) for time-series spanning a few decades. Certainly, the presence of b_P can increase the uncertainty of the linear regression result (b). Thus, the 95 per cent CI for the trend (b) could be estimated by $1.96 \times \text{SE}_{bc}$, plus the absolute value of the linear trend (b_P) of P_i:

$$b_{95\,\text{per cent}CI} \approx 1.96 \times \text{SE}_{bc} + |b_P|. \tag{13}$$

Fig. 7 illustrates the values of b_P for 1 160 TG data sets globally distributed, which were selected according to the criteria discussed in the following section. The 95 per cent CI for each data set is also plotted for comparison. The results show that, in general, the contribution of b_P to the 95 per cent CI is negligible. For data with a time span of less than 30 yr, b_P can be remarkable (>0.2 mm yr^{-1}); however, for TG data spanning 30 yr or more, the absolute value of b_P is typically negligible (<0.1 mm yr^{-1}).

2.4 Python module: TG_rate_95CI.py

To facilitate the implementation of the methodology proposed in this paper, we have developed a Python module named TG_Rate_95CI.py. This module has been integrated into the Python libraries as an internal function and can be easily installed on a user's computer with the Package Installer for Python (pip). Detailed instructions and an example main program that calls the function can be found on the Python Package Index (PyPi) website at https://pypi.org/project/TG-Rate-95CI. This module enables researchers and engineers with limited coding experience to conduct advanced TG data analysis. Instead of spending hours on coding, they can focus on using the MSL time-series in their respective fields. For advanced users who wish to modify or improve our methods, the source code and detailed instructions can be found on our GitHub site at https://github.com/bob-Github-2020/TG_Rate_95CI. The module outputs many key components, including the original MSL time-series, the linear trend, ACF, the long-period component (gap-filled), the periodic component (gap-filled), the residual time-series (gap-filled) and key parameters used to calculate the 95 per cent CI. An example output for the decomposition can be seen in Fig. 3.

3 RESULTS AND DISCUSSION

3.1 An empirical model for projecting the 95 per cent CI

As of 2021, PSMSL releases monthly MSL data from approximately1550 TG stations operated by numerous TG networks worldwide (PSMSL 2022a). This study selected monthly MSL data (as the end of 2021) that have an observational time spanning longer than 10 yr with data gaps less than 30 per cent of the total observational period. In our analysis, we employed linear regression, assuming a linear change over time. Consequently, we excluded sites with anomalous shifts associated with vertical land surface movements (e.g. co-seismic, post-seismic land surface deformation, anthropogenic subsidence and volcanic activities) and unexplained instrumental datum shifts, as well as those displaying obvious nonlinear features. It is crucial to recognize that data shifts in TG time-series should be approached with caution when conducting long-term sea-level change studies, as they have the potential to introduce errors in estimating sea-level change rates. Ultimately, we selected 1160 TG data sets for this study (Fig. 8), and calculated the rates of MSL changes and their uncertainties using the Python module. Figs 8(a)–(c) show the time span (T), linear trend (b) and 95 per cent CI of these selected TG data sets, respectively. These linear trends are not corrected for local land movement.

The colour patterns presented in Figs 8(a) and (c) reveal a strong correlation between the time span (T) and the uncertainty (95 per cent CI). Fig. 9 depicts the 95 per cent CI of the relative MSL rates versus the total observational time span (T) in both a log–log and a linear plot. The log–log plot reveals a linear relationship between log(95 per centCI) and log(T), indicating a power-law relationship between the 95 per cent CI and T. The $\pm$ 95 per cent CI can be fitted best by a least-squares regression line, as shown below:

$$95\text{per centCI} = 179.8T^{-1.29}, \tag{14}$$

where T is the year range of the time-series in years, and the $\pm$ 95 per cent CI is measured in millimetres per year. The 95 per cent CI tends to decrease rapidly with the increase of time span. Fig. 9(b) further reveals that the 95 per cent CI estimates vary widely, particularly for the data sets spanning less than 30 yr. The Python module also outputs the projected 95 per cent CI estimates based on eq. 14 (see Fig. 3a). If the calculated 95 per cent CI for a particular site is significantly larger than the projected value (e.g. > 0.5 mm yr^{-1}), it may be an indication that the site is unusual and warrants further investigation.

As mentioned previously, TG data sets with data gaps greater than 30 per cent of the total observation period were excluded from the development of the global model (eq. 14). To investigate the impact of data gaps on 95 per cent CI estimates, we examined MSL time-series with data gaps between 20 and 30 per cent of their operational periods, selecting from the 1160 globally distributed TG stations (Fig. 8). Of these stations, 115 fell within this data gap range. We have found that these data sets with data gaps between 20 to 30 per cent of their operational period did not exhibit a statistically larger 95 per cent CI than those with smaller data gaps, as shown in Fig. 10. However, it is crucial to keep in mind that extensive gaps in MSL time-series, exceeding a few years, may include shifts resulting from instrument or datum (reference benchmarks) changes that were inadequately documented. Therefore, researchers should exercise prudence when utilizing TG data that contains significant data gaps in their analyses.

The empirical model (eq. 14) provides a powerful tool that can be used to determine the optimal observational time span needed to achieve a desired level of uncertainty in the estimation of sea-level rise rate or coastal subsidence rate from TG data. It has a wide range of applications, from coastal infrastructure planning to climate research. For example, engineers and planners can use it to determine the minimum length of TG data required to estimate the rate of land submergence and its associated uncertainty for coastal infrastructure planning and real estate investment. In addition, the empirical model can be a useful educational tool in Earth science to illustrate the importance of considering the length of the observational time span when analysing geophysical data trends. Overall, the empirical equation provides valuable guidance for making informed decisions and understanding the uncertainties associated with sea-level rise and coastal subsidence.

3.2 UH versus PSMSL solutions

PSMSL publishes the rate and uncertainty from approximately 800 TG stations (as of 2021) which were selected from a pool of around 1550 global TG stations. The selection criteria include a continuous measurement period of over 30 yr and data gaps of less than 30 per cent of the entire time span. PSMSL has flagged certain stations for quality issue, and trends are not calculated for these stations. In PSMSL's processing, the TG time-series is broken down into three components: a linear trend, a seasonal component and a noise component. The noise component is modelled using a synthetic model with three stochastic parameters, an amplitude and a white noise. The trend is fitted using an Integrated Generalized Gauss Markov stochastic model (PSMSL 2022b), and the uncertainty is determined based on the modelled noise.

For stations with large data gaps exceeding a decade, PSMSL used the longest available portion of the data set before or after the gap, whereas the UH method tried to fill the gap. For a few stations with significant gaps, the data sets used in the UH and PSMSL processing differed substantially. To ensure consistency, we selected 770 data sets from these 800 PSMSL dat asets for which both UH and PSMSL methods used the same data. In Fig. 11(a), we compare the solutions (95 per cent CI) obtained by PSMSL and UH for the

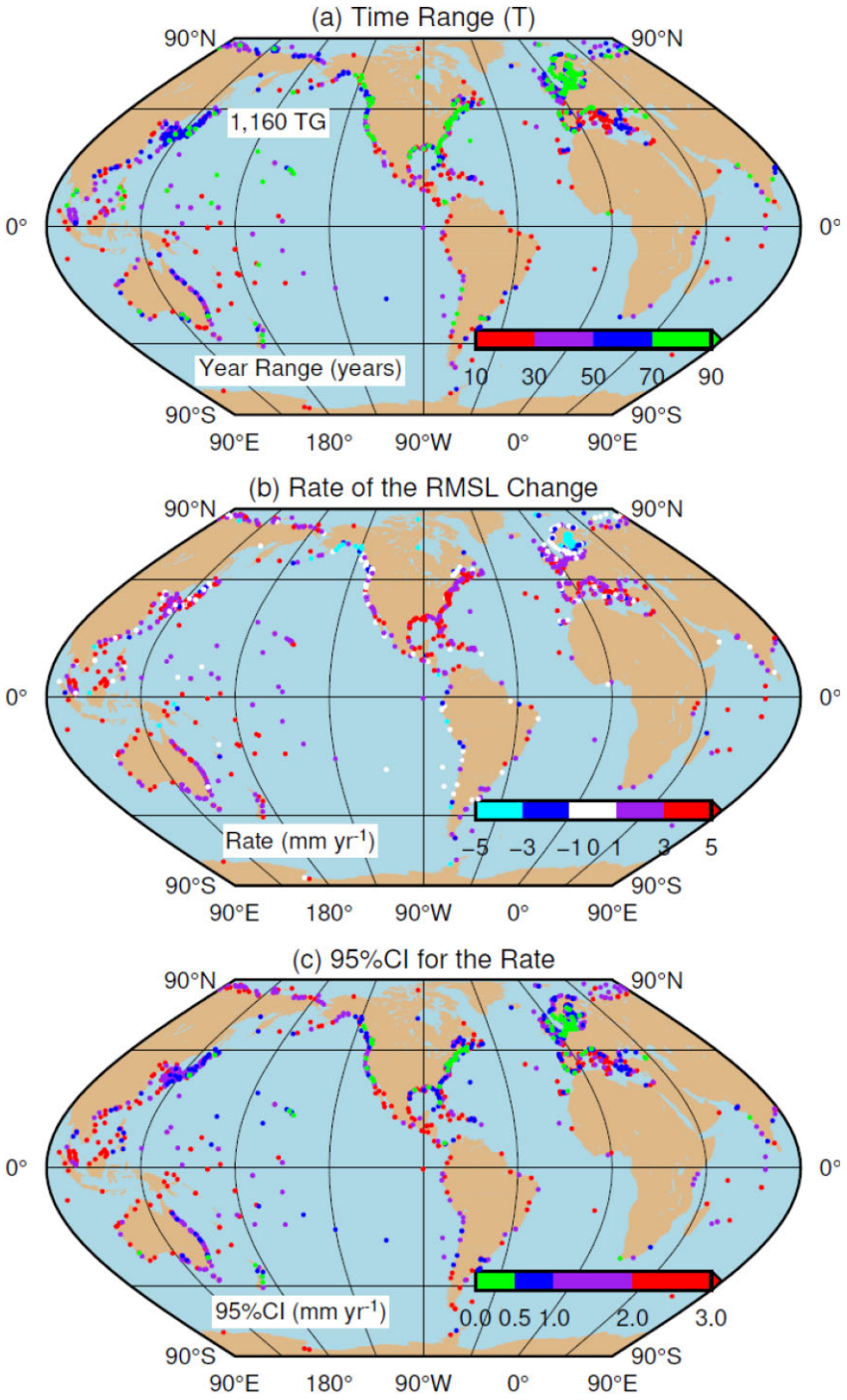

Figure 8. Maps depicting the locations of 1160 long-term TG stations selected for developing the global model (eq. 14). (a) The colour showing the time range of observational history; (b) the colour showing the rate of the relative sea-level (RSL) change and (c) the colour indicating the range of 95 per cent CI for the rate.

770 TG data sets. The distribution of scattered data points indicates that the solutions from the two methods are comparable. However, the UH solution has a smaller scatter. The regression lines suggest that the 95 per cent CI estimates obtained from the UH method are statistically larger by about 0.2 mm yr^{-1} than those from the PSMSL method for data sets with a time range of less than approximately 50 yr. For data sets with a time span longer than 50 yr, the 95 per cent CI estimates from the UH and PSMSL methods are the same.

3.3 UH versus NOAA solutions

NOAA releases monthly MSL data, seasonally adjusted, for about 135 TG stations along the U.S. coasts with an observational time span of 30 yr or longer (NOAA 2022a). These stations are located on the U.S. Atlantic and Pacific coasts, the Gulf of Mexico, Hawaii, Alaska and islands in the Atlantic and Pacific Oceans. For each station, NOAA publishes the rate and its uncertainty (rate ± 95 per cent CI) using a minimum time span of 30 yr (NOAA 2022b).

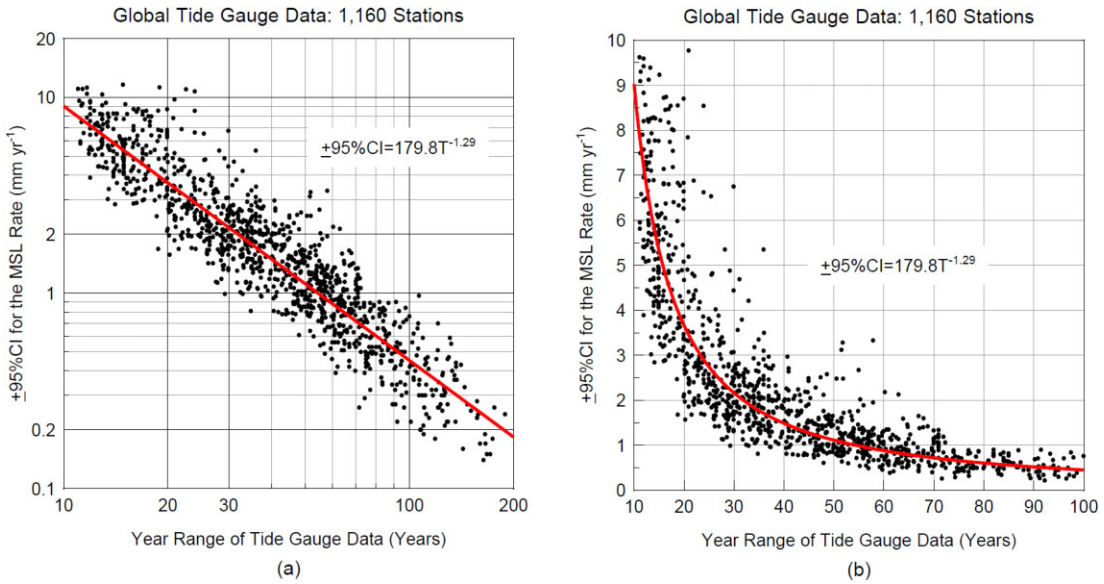

Figure 9. (a) A log–log plot showing the correlation between the 95 per cent CI and the year range (T) of global TG data and (b) a linear plot depicting the power-law relationship between the 95 per cent CI and T.

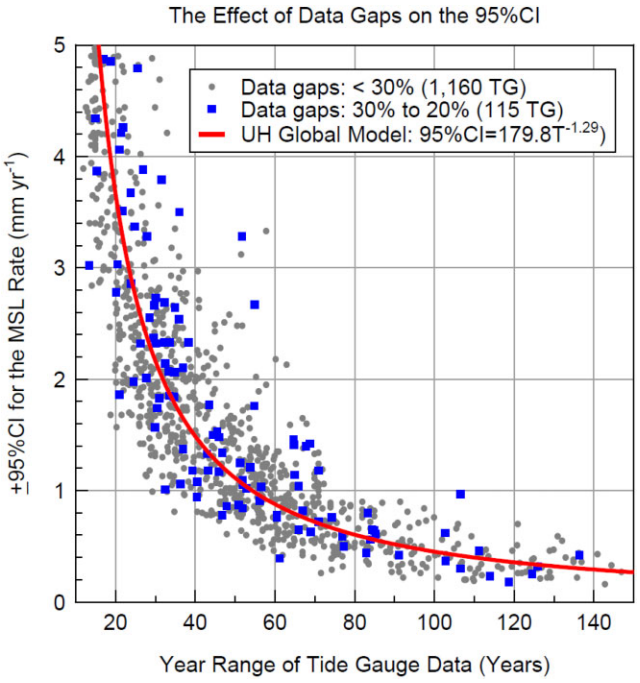

Figure 10. Comparisons of 115 TG data sets with data gaps between 20 to 30 per cent of their observation time span to those 1160 global TG data sets with less than 30 per cent data gaps.

In this study, we processed all these data with the Python module TG_Rate_95CI.py. Fig. 11(b) compares the UH and NOAA solutions (95 per cent CI) for these 135 NOAA data sets. The regression lines suggest that, statistically, the UH solution is about 0.1–0.2 mm yr^{-1} larger than the NOAA solution. The figure also includes the UH global model (eq. 14), developed based on 1160 TG data sets downloaded from PSMSL. Notably, the UH global model appears to be about 0.2 mm yr^{-1} higher than the regression line obtained from the NOAA data. This indicates that NOAA's pre-processing, which involves removing seasonal cycles, has slightly reduced the uncertainty of the linear trend. We suggest that users focusing on regional sea-level changes and coastal subsidence along the U.S. coasts may consider using the NOAA data. For meticulous users, it is recommended to check both the NOAA and PSMSL data. NOAA periodically updates its data sets for quality control purposes, including revisions made to historical data that may not be reflected in the PSMSL database (as confirmed through email correspondence with Andrew Matthews at PSMSL and Jerry Hovis at NOAA).

3.4 Spatial variation of the 95 per cent CI

The spatial variability of the uncertainty for the rate of sea-level changes has been realized in previous investigations (e.g. Zervas 2009; Royston *et al.* 2018). For instance, NOAA has noted that the 95 per cent CI estimates for stations along the Atlantic Ocean, Eastern Gulf of Mexico and Caribbean Sea are smaller than those along the Pacific Ocean, Western Gulf of Mexico and Bermuda (Zervas 2009). In general, areas with high variance in sea-level changes and strong temporally correlated noises exhibit significant 95 per cent CI estimates.

Fig. 12 illustrates the 95 per cent CI at TG sites along the coasts of the U.S., Japan, Australia, the U.K. and Finland. The analysis shows that the 95 per cent CI for TG sites located on the Finland and Japan coasts are larger than the global average illustrated by the UH Global Model (eq. 14). On the other hand, the 95 per cent CI estimates on the Australian coasts are generally smaller than the global average. In contrast, the 95 per cent CI along the coasts of the U.S. and the U.K. are comparable to the global average. Although the detailed investigation of the spatial variability of the rate uncertainty is beyond the scope of this paper, the Python module developed in this study provide a powerful tool for further research on this topic.

3.5 Application: determining the 95 per cent CI for the ASL rate

The ASL rate with respect to a global geodetic reference frame can be obtained by:

$$\mathrm{ASL} = \mathrm{RSL} + \mathrm{VLM}. \tag{15}$$

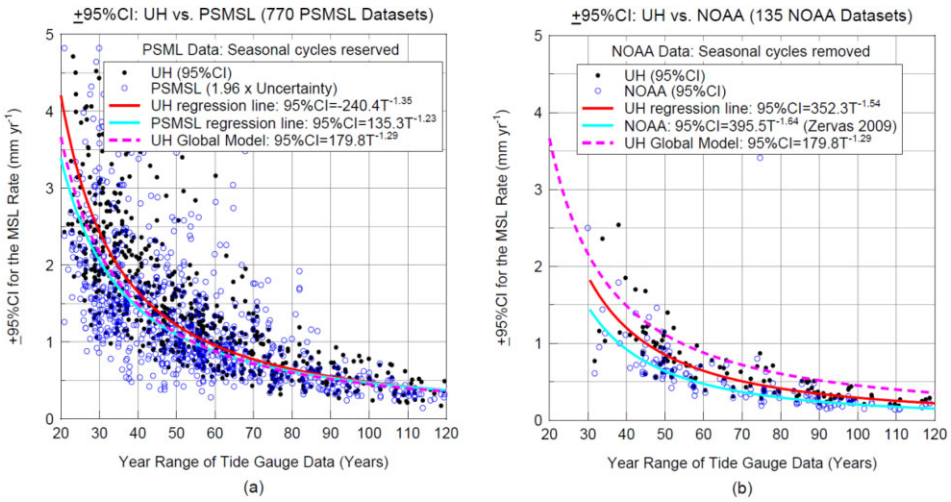

Figure 11. (a) Comparisons of the PSMSL and UH solutions (95 per cent CI) for 770 TG data sets released by PSMSL and (b) comparisons of the NOAA and UH solutions (95 per cent CI) for 135 TG data sets along the U.S. coasts released by NOAA.

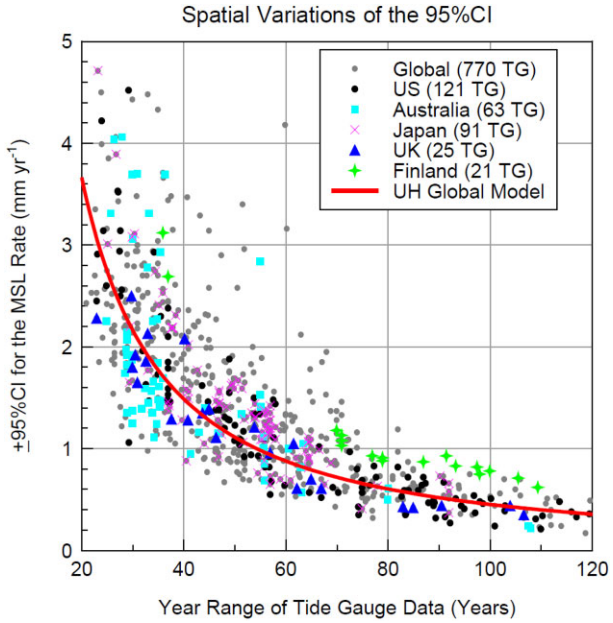

Figure 12. Plot depicting the spatial variability of the 95 per cent CI.

The uncertainties in the rates of VLM and RSL are independent but jointly contribute to the overall uncertainty in the ASL change rate estimate. Assuming that the uncertainties in the VLM and RSL rates are primarily governed by a normal (or Gaussian) distribution, the uncertainty for the rate of ASL change can be estimated using the following equation:

$$E_{\mathrm{ASL}} = \sqrt{(E_{\mathrm{VLM}})^2 + (E_{\mathrm{RSL}})^2}. \tag{16}$$

To estimate the 95 per cent CI for the linear trend of VLM from daily GNSS time-series, the empirical model (95 per cent CI $= 5.2T^{-1.25}$) developed by Wang (2022) can be used. This model is based on daily displacement time-series from 9700 GNSS stations distributed worldwide. Fig. 13 shows the empirical models proposed to project the 95 per cent CI of VLM and RSL change rates based on daily GNSS data and monthly TG data, respectively. To achieve a 1 mm yr^{-1} uncertainty for the rates of VLM and RSL, it typically requires about five years of GNSS data and 50 yr of TG data. However, this length of time span may still result in a larger than 1 mm yr^{-1} uncertainty for the ASL change rate. To retain submillimetre uncertainty ($<$ 1 mm yr^{-1}) in the ASL change rate, a minimum of 7 yr of GNSS data and 60 yr of TG data are recommended, and to achieve a 0.5 mm yr^{-1} uncertainty for the ASL change rate, approximately 10 yr of GNSS data and 80 yr of TG data are recommended.

On the coast of Galveston Island, both TG data sets show the same rate of RSL change, approximately 6.6 mm yr^{-1} (as shown in Fig. 1). Nevertheless, the longer data set (Pier 21, 1908–2021) retains a smaller uncertainty. Close to the TG sites, there are several continuous GNSS stations (also shown in Fig. 1a), which reveal an ongoing VLM rate of -3 to -4 mm yr^{-1} relative to the International GNSS Service Reference Frame 2014 (IGS14, Rebischung *et al.* 2016). Among these GNSS stations, TXGA has the longest history (16 yr: 2005–2021) and provides the most reliable VLM rate as of 2021: -3.67 ± 0.22 mm yr^{-1} with respect to IGS14. According to Zhou *et al.* (2021), the GNSS-derived VLM is dominated by natural subsidence, which remains constant over a geological timescale. Using a combination of TG and GNSS data, the 95 per cent CI for the ASL change rate at Galveston Island over the past century (1908–2021) can be estimated as: $\sqrt{0.41^2 + 0.22^2} = 0.47$ mm yr^{-1}. This uncertainty for the site-specific ASL change rate is similar to the uncertainty reported by the latest IPCC report for the GMSL rate, which is 1.7 $\pm$ 0.4 mm yr^{-1} between 1901 and 2018 (IPCC 2021). Note that the uncertainty reported by IPCC is quantified by a 90 per cent CI, whereas the 90 per cent CI of $\pm$ 0.4 mm yr^{-1} is comparable to a 95 per cent CI of $\pm$ 0.5 mm yr^{-1}. The IPCC is commonly perceived as a leading authority on sea-level change and climate science, and as such, the agreement between the uncertainty estimates (95 per cent CI) of ASL change rates from the empirical model proposed in this study with the IPCC estimate is particularly noteworthy.

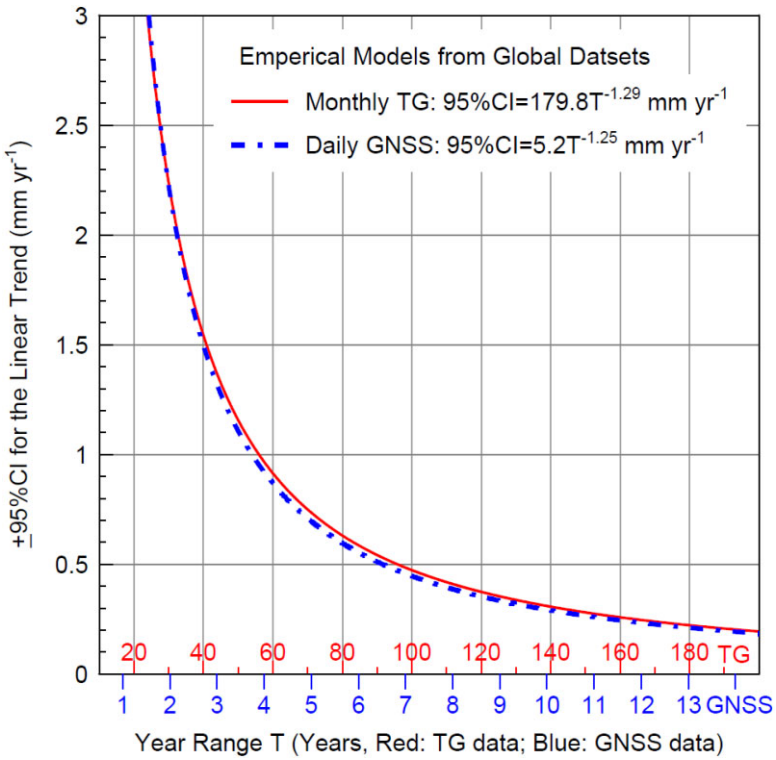

Figure 13. Comparison of empirical models for estimating the 95 per cent CI for the rates of VLM and relative sea-level (RSL) change. The model for daily GNSS time-series is based on a regression line obtained according to 9700 global GNSS data sets (Wang 2022), while the model for monthly MSL time-series is based on a regression line obtained according to 1160 TG data sets.

4. CONCLUSIONS

This study proposes a rigorous approach for calculating the ± 95 per cent CI for the RSL change rates derived from monthly MSL time-series that are affected by time-correlated noises. The methodology involves decomposing the monthly MSL time-series into three components: a linear trend, a periodic component and a noise time-series. By examining the ACF of the noise time-series, a N_{eff} is determined, which results in a reliable estimate of the rate uncertainty for RSL change. The study shows that there is an inverse power-law relationship between the 95 per cent CI and the time span (T) of the TG time-series. To predict the 95 per cent CI, an empirical model is established based on 1160 globally dispersed TG data sets, which yields 95 per cent CI $= 179.8T^{-1.29}$. According to the empirical model, a continuous monthly TG data set of 20 yr may only attain a 95 per cent CI of 3–5 mm yr^{-1}, while a 30-yr TG data may yield approximately 2 mm yr^{-1} 95 per cent CI. To achieve a more precise 95 per cent CI of submillimetre per year, roughly 60 yr of continuous TG observations are necessary. For an even more precise 95 per cent CI of 0.5 mm yr^{-1}, around 80 yr of monthly MSL observations are required.

The 95 per cent CI estimates derived from the UH methodology are generally consistent with those of the PSMSL and NOAA methods. Statistically, the UH estimates are about 0.1–0.2 mm yr^{-1} larger than the PSMSL and NOAA solutions for TG data sets shorter than approximately 50 yr and are the same for the longer data sets. However, the UH methodology may be more accurate than the other methods because it accounts for multiperiodicities as the deterministic portion, including seasonal, multiyear and multidecadal variations in addition to annual and half-annual periods. For shorter data sets (e.g. $<$ 50 yr), these periodic signals could have a significant impact on the linear trends. The UH method also separately accounts for the effects of deterministic and stochastic portions on the linear trend, and is more straightforward than other methods, estimating the effective sample size (N_{eff}) using only the ACF of the noise time-series without complex modelling or parameter adjustments. Additionally, the UH methodology has been implemented as a Python module that is easy to use, install, and adaptable for a wide range of applications. Considering the broad applications of TG data in science and engineering and the popularity of Python as a programming language for the young generation (graduate students), the UH methodology, the empirical model and the Python module have the potential for broad applications in coastal environmental and engineering, global sea-level rise and climate change studies and Earth science education.

ACKNOWLEDGMENTS

I would like to express my sincere gratitude to the three anonymous reviewers who provided valuable insights and thoughtful comments on this study. I am grateful to Andrew Matthews at PSMSL and Jerry Hovis at NOAA for their helpful responses to my inquiries regarding the difference between PSMSL and NOAA data. I would also like to extend my appreciation to Dr Linqiang Yang (University of Hawaii at Manoa), Dr Xiao Yu and Mr Kuan Wang (University of Houston) for their assistance in testing the module on their computers with different operating systems, including Linux, Mac OS, and Microsoft Windows. Lastly, I would like to acknowledge the utilization of GMT software, as described in Wessel *et al.* (2013), for creating Figs 1(a) and 8.

DATA AVAILABILITY

The PSMSL data can be accessed from the website https://psmsl.org/data/. The NOAA data can be accessed from the NOAA Center for Operational Oceanographic Products and Services, https://tidesandcurrents.noaa.gov/sltrends/sltrends.html (for seasonally adjusted data). For the Python module TG_Rate_95CI.py, it can be found in the Python Package Index (PyPI) at https://pypi.org/project/TG-Rate-95CI/. For those interested in accessing the source codes and a detailed document, they are available on the author's GitHub site https://github.com/bob-Github-2020/TG_Rate_95CI.

CONFLICT OF INTEREST

The author has no conflict of interest to declare.

REFERENCES

Agnew, D.C., 1992. The time-domain behaviour of power-law noises, *Geophys. Res. Lett.,* **19**(4), 333–336.

Beran, J., 1992. Statistical methods for data with long-range dependence, *Stat. Sci.,* **7**(4), 404–416.

Bos, M.S., Williams, S.D.P., Araujo, I.B. & Bastos, L., 2014. The effect of temporal correlated noise on the sea level rate and acceleration uncertainty, *Geophys. J. Int.,* **196**(3), 1423–1430.

Box, G.E.P., Jenkins, G.M. & Reinsel, G.C., 2008. *Time Series Analysis, Forecasting and Control*(4th ed.). Hoboken, NJ: Wiley. ISBN 9780470272848.

Burgette, R.J., Watson, C.S., Church, J.A., White, N.J., Tregoning, P. & Coleman, R., 2013. Characterizing and minimizing the effects of noise in tide gauge time series: relative and geocentric sea level rise around Australia, *Geophys. J. Int.,* **194**(2), 719–736.

Church, J.A. & White, N.J., 2011. Sea-level rise from the late 19th to the early 21st century, *Surv. Geophys.,* **32,** 585–602.

Cleveland, W.S., 1981. LOWESS: a program for smoothing scatterplots by robust locally weighted regression, *Am. Stat.,* **35**(1), 54.

Cornelison, B. & Wang, G., 2022. GNSS_Vel_95CI.py: a Python module for calculating the uncertainty of GNSS-derived site velocity, *J. Surv. Eng.,* 2023, **149**(1), 06022001.

Dangendorf, S., Rybski, D., Mudersbach, C., Müller, A., Kaufmann, E., Zorita, E. & Jensen, J., 2014. Evidence for long-term memory in sea-level, *Geophys. Res. Lett.,* **41,** 5530–5537.

Faouzi, J. & Janati, H., 2020. pyts: a python package for time series classification, *J. Mach. Learn. Res.,* **21**(46), 1–6.

Geyer, C.J., 1992. Practical Markov chain Monte Carlo, *Stat. Sci.,* **7**(4), 473–483.

Golyandina, N. & Zhigljavsky, A., 2020. *Singular Spectrum Analysis for Time Series*. Springer Berlin Heidelberg, January 2020. https://doi.org/10.1007/978-3-662-62436-4. ISBNs: 978-3-66-262435-7, 978-3-66-262436-4

Hamlington, B.D., Frederikse, T., Nerem, R.S., Fasullo, J.T. & Adhikari, S., 2020. Investigating the acceleration of regional sea level rise during the satellite altimeter era, *Geophys. Res. Lett.,* **47,** e2019GL086528.

Harrison, C.G.A., 2002. Power spectrum of sea level change over fifteen decades of frequency, *Geochem. Geophys. Geosyst.,* **3**(8), 10047.

Hay, C.C., Morrow, E., Kopp, R.E. & Mitrovica, J.X., 2013. Estimating the sources of global sea level rise with data assimilation techniques, *Proc. Natl. Acad. Sci.,* **110**(Suppl. 1), 3692–3699.

Holgate, S.J. *et al.*, 2013. New data systems and products at the Permanent Service for Mean Sea Level, *J. Coastal Res.,* **29**(3), 493–504. http://doi.org/10.2112/JCOASTRES-D-12-00175.1.

Hughes, C.W. & Williams, S.D.P., 2010. The color of sea level: importance of spatial variations in spectral shape for assessing the significance of trends, *J. geophys. Res.,* **115**(C14), 10048.

Kass, R.E., Carlin, B.P., Gelman, A. & Neal, R., 1998. Markov chain Monte Carlo in practice: a roundtable discussion, *Am. Stat.,* **52**(2), 93–100.

Kermarrec, G., Lösler, M., Guerrier & Schön, S., 2022. The variance inflation factor to account for correlations in likelihood ratio tests: deformation analysis with terrestrial laser scanners. *J. Geod.,* **96**(86), https://doi.org/10.1007/s00190-022-01654-5.

Langbein, J., 2004. Noise in two-color electronic distance meter measurements revisited, *J. geophys. Res.,* **109,** B04406. https://doi.org/10.1029/2003JB002819

Langbein, J., 2012. Estimating rate uncertainty with maximum likelihood: differences between power-law and flicker-random-walk models, *J. Geod.,* **86**(9), 775–783.

Langbein, J. & Johnson, H., 1997. Correlated errors in geodetic time series: implication for time dependent deformations, *J. geophys. Res.,* **102**(B1), 591–603.

Nerem, R.S., Chambers, D., Choe, C. & Mitchum, G.T., 2010. Estimating mean sea level change from the TOPEX and Jason Altimeter missions, *Mar. Geod.,* **33**(1), 435–446

NOAA, 2022a. Sea level trends, https://tidesandcurrents.noaa.gov/sltrends/ (last accessed 18 January 2023).

NOAA, 2022b. U.S. Linear Relative Sea Level (RSL) trends and 95% Confidence Intervals (CI) in mm/year and in ft/century. https://tidesandcurrents.noaa.gov/sltrends/mslUSTrendsTable.html (last accessed 18 January 2023).

Peng, D., Hill, E.M., Meltzner, A.J. & Switzer, A.D., 2019. Tide gauge records show that the 18.61-year nodal tidal cycle can change high water levels by up to 30 cm, *J. geophys. Res.: Oceans,* **124**(1), 736–749.

PSMSL, 2022a. RLR monthly tide gauge data, http://www.psmsl.org/data/obtaining/ (last accessed 18 January 2022).

PSMSL, 2022b. Methods used for fitting trends, https://psmsl.org/products/trends/methods.php (last accessed 18 January 2023).

Qiao, X., Chu, T., Tissot, P., Louis, J. & Ali, I., 2022. Land subsidence estimation with tide gauge and satellite radar altimetry measurements along the Texas Gulf coast, USA, *IEEE Geosci. Remote Sens. Lett.,* **19,** 1–5.

Rebischung, P., Altamimi, Z., Ray, J. & Garay, B., 2016. The IGS contribution to ITRF2014, *J. Geod.,* **90**(7), 611–630.

Royston, S., Watson, C.S., Legrésy, B., King, M.A., Church, J.A. & Bos, M.S., 2018. Sea-level trend uncertainty with Pacific climatic variability and temporally-correlated noise, *J. geophys. Res.: Oceans,* **123,** 1978–1993.

Snay, R. *et al.*, 2007. Using global positioning system derived crustal velocities to estimate rates of absolute sea level change from North American tide gauge records, *J. geophys. Res.,* **112**(B4), B04409. https://doi.org/10.1029/2006JB004606.

Straatsma, T.P., Berendsen, H.J.C. & Stam, A.J., 1986. Estimation of statistical errors in molecular simulation calculations, *Mol. Phys.,* **57**(1), 89–95.

Taubenheim, J., 1974. On the significance of the autocorrelation of statistical tests for averages, mean-square deviations and superposed epochs, *Gerlands Beitr. Geophys.,* **83,** 121–128.

Thiébaux, H.J. & Zwiers, F.W., 1984. The interpretation and estimation of effective sample size, *J. Appl. Meteorol. Climatol.,* **23**(5), 800–811.

Thompson, M.B., 2010. *A Comparison of Methods for Computing Autocorrelation Time*. Technical Report No. 1007, Department of Statistics, University of Toronto. https://arxiv.org/pdf/1011.0175.pdf.

Wang, G., 2022. The 95% confidence interval for the GNSS-derived site velocities, *J. Surv. Eng.,* **148**(1), 04021030. https://doi.org/10.1061/(ASCE)SU.1943-5428.0000390

Wang, G., Zhou, X., Wang, K., Ke, X., Zhang, Y., Zhao, R. & Bao, Y., 2020. GOM20, a stable geodetic reference frame for subsidence, faulting, and sea-level rise studies along the coast of the Gulf of Mexico, *Remote Sens.,* **12**(3), 350. https://doi.org/10.3390/rs12030350

Wessel, P., Smith, W.H., Scharroo, R., Luis, J. & Wobbe, F., 2013. Generic mapping tools: improved version released, *Eos,* **94**(45), 409–410.

Wilks, D.S., 2006. *Statistical Methods in the Atmospheric Sciences*. 2nd edn Cambridge, MA: Academic

Williams, S.D.P., 2008. CATS: GPS coordinate time series analysis software, *GPS Solut.*, **12**(2), 147–153.

Yang, L. & Francis, O., 2019. Sea-level rise and vertical land motion on the Islands of Oahu and Hawaii, Hawaii, *Adv. Space Res.,* **64**(11), 2221–2232.

Yu, J. & Wang, G., 2016. Introduction to the GNSS geodetic infrastructure in the Gulf of Mexico Region, *Surv. Rev.,* **47**(352), 51–65. http://doi.org/10.1080/00396265.2015.1108069

Zervas, C. 2009. *Sea Level Variations of the United States 1854-2006*. NOAA Technical Report NOS CO-OPS 053. NOAA National Ocean Service Center for Operational Oceanographic Products and Services, https://www.tidesandcurrents.noaa.gov/publications/Tech_rpt_ 53.pdf.

Zervas, C., Gill, S. & Sweet, W., 2013. *Estimating vertical land motion from long-term tide gauge records,* NOAA Technical Report NOS CO-OPS 065. http://dx.doi.org/10.25607/OBP-141

Zhang, X. & Church, J.A., 2012. Sea-level trends, interannual and decadal variability in the Pacific Ocean, *Geophys. Res. Lett.,* **39,** L21701. https://doi.org/10.1029/2012GL053240

Zhou, X., Wang, G., Wang, K., Liu, H., Lyu, H. & Turco, M.J., 2021. Rates of natural subsidence and submergence along the Texas coast derived from GPS and tide gauge measurements (1904–2020), *J. Surv. Eng.,* **147**(4), 04021020, https://doi.org/10.1061/(ASCE)SU.1943-5428.0000371.

IPCC, 2021. Summary for policymakers. In: *Climate Change 2021: The Physical Science Basis. Contribution of Working Group I to the Sixth Assessment Report of the Intergovernmental Panel on Climate Change*[Masson-Delmotte, V., *et al.*, Cambridge University Press, Cambridge, United Kingdom and New York, NY, USA, pp. 3–32, http://doi.org/10.1017/9781009157896.001.

Zervas, C., 2001. Sea level variations of the United States 1854-1999. NOAA Technical Report NOS CO-OPS 036. NOAA National Ocean Service Center for Operational Oceanographic Products and Services., https://https://repository.library.noaa.gov/view/noaa/14663/noaa_14663_DS1.pdf.